Photoabsorption spectra of small Na clusters: TDHF and BSE versus CI and experiment

C. H. Patterson
School of Physics, Trinity College Dublin, Dublin 2, Ireland

(Received 2 February 2019; published 30 April 2019)

Time-dependent Hartree-Fock (TDHF) and Bethe-Salpeter equation (BSE) methods are benchmarked against configuration interaction (CI) calculations of excitation energies and photoabsorption cross-sections for small closed shell sodium clusters with up to six atoms in several low-energy configurations. The mean absolute deviation of lowest excitation energies of each symmetry in these clusters for TDHF or BSE calculations from CI results is about 0.1 eV. The Thomas-Reiche-Kuhn (TRK) sum rule is satisfied to within numerical accuracy for both TDHF and BSE calculations, however, the Tamm-Dancoff approximations applied to either method for these systems yield optical cross-sections which grossly violate the TRK sum rule. TDHF and BSE calculations for photoabsorption cross-sections of Na_8 and Na_{20} clusters are compared to experiment and found to be in good agreement. A feature in the cross-section of Na_{20} above 4 eV is found to be caused by a large density of optical transitions rather than an incipient volume plasmon with a short lifetime.

DOI: 10.1103/PhysRevMaterials.3.043804

I. INTRODUCTION

The *GW* and Bethe-Salpeter equation (BSE) many-body methods have been successfully applied to calculation of particle, hole and optical excitation spectra of organic molecules [1–4] and solids [5–8]. Here we report time-dependent Hartree-Fock (TDHF) and *GW*/BSE calculations of photoabsorption cross-sections for a set of closed shell sodium clusters (Na_2, Na_3^+, Na_4, Na_5^+, Na_6, Na_8, and Na_{20}) in a range of low-energy configurations. These methods have been benchmarked against coupled cluster (CC) methods for organic molecules [2,3,9,10]. For solids, these methods have generally been benchmarked against experiment, as they are commonly the most accurate method available in that case. Comparisons between configuration interaction (CI) and *GW*/BSE methods have been made for Hubbard hamiltonian systems ranging from metallic to insulating [11].

Here we benchmark TDHF and G_oW_o/BSE methods against full CI (FCI) for Na_2 to Na_4 and against CI with up to quadruple excitations (QCI) for Na_6 using the atomic coordinates and basis set used for CI calculations on these systems by Priya and Shukla [12]. Perturbative G_oW_o calculations are commonly performed using density functional theory (DFT) Kohn-Sham states as a starting point, so that the exchange-correlation potential is replaced by the static Fock exchange and the dynamically screened Coulomb interaction. Here we use a Hartree-Fock (HF) starting point which includes the Fock exchange. TDHF and G_oW_o/BSE approaches predict similar excitation energies for Na clusters, which is not the case, for example, in polyacene organic systems [13]. This may be caused by the low-electron density, few-electron nature of these systems which results in limited screening of the Coulomb interaction. TDHF is equivalent to the RPA method including exchange and TDHF-TDA is equivalent to the CI singles (CIS) method in quantum chemistry.

We also report TDHF and G_oW_o/BSE calculations for Na_8 and Na_{20} clusters. Na_8 clusters have been studied previously using CI methods [14]. Early theoretical work on optical properties of Na clusters used spherical or ellipsoidal jellium models with the time-dependent local density approximation (TDLDA) [15–22], time-dependent density functional theory (TDDFT) [23–26] or RPA with exchange (TDHF) [16,17,27–30]. More recently G_oW_o calculations on Na_4 [31–33] and Na_9^+ and Na_{21}^+ [33] and Bethe-Salpeter equation (BSE) calculations on Na_4 [31,32] and closed shell neutral [34] and positive ion [35] Na_n clusters with $n = 2$ to $n = 8$ have been reported. Double ionization energy spectra of closed shell neutral clusters [36] have been investigated by a $GW + T$ matrix approach and the importance of vertex corrections in Na_3 [37] has been investigated.

Small Na clusters are few-electron, low-electron density systems. Approximations, which work effectively for covalently bonded organic molecules, for example, may or may not be successful in these systems. One of the surprising outcomes of this work is that the Tamm-Dancoff approximation (TDA), which is generally acknowledged to be faithful to the full BSE method in solids [38] and successful in predicting experimental band gaps and absorption spectra in gapped periodic systems, grossly fails to satisfy the Thomas-Reiche-Kuhn (TRK) sum rule [39–41] in these systems. In contrast, both TDHF and BSE approaches typically satistfy the TRK rule to within 2% (which reflects the numerical accuracy of the method). This is as expected as both TDHF and BSE are conserving approximations, in the sense of Baym and Kadanoff [42]. The TRK sum rule failure of the TDA in this case is mainly overestimation of transition dipole moments for higher energy, dipole active transitions and it is by a factor of three or more in the largest clusters studied. Reasons for this are considered below. Failure of the TDA to a more limited extent in BSE calculations has been noted previously in azobenzene and carbon nanotubes [43]. Sum rules within the random phase approximation (RPA) applied to Na clusters have been discussed in detail by Reinhard and coworkers [44].

Photoelectron detachment, photoabsorption and static polarizabilities of simple metal clusters have been comprehensively reviewed by de Heer [45]. Early studies of abundances of Na_n clusters for $n = 4$ to 100, showed greater abundances at $n = 8$, 20, 40, 58, and 92 [46], whose stability was associated with electronic shell filling. Measurements of electric polarizabilities of Na_n clusters in the range up to $n = 40$ [47] and up to $n = 200$ [48] showed reduced static polarizability at $n = 8$ and $n = 20$, confirming their stable electronic configurations. Subsequently, photoabsorption measurements of cold, neutral [49–51] and positively charged [52] sodium clusters were reported for clusters with up to 8 [53], 40 [50,51,54], or 64 [52] atoms. The temperature dependence of optical spectra of Na_n^+ ions with $n = 4$, 7, and 11 was measured in the temperature range to 380 K [55], which showed that clusters adopted a spheroidal, liquid structure at this temperature. Later, Schmidt and coworkers reported the temperature dependence of optical spectra of sodium cluster positive ions [52,56].

Atomic structures of small sodium clusters have been determined using density functional theory (DFT) in the local density approximation (LDA) [20,57,58] and a generalized gradient approximation (GGA) [58]. Alternatively, HF [59–61] and CI methods [14,59,62–64] have been used for structure determination and calculation of optical spectra. Various many-body potential approaches have also been applied to structure determination, especially of larger clusters [65]. More recently, a particle swarm optimization technique combined with a hybrid density functional was used to obtain structures of Na_n clusters with 10 to 25 atoms [66]. An *ab initio* molecular dynamics approach has been used to study melting of Na clusters [67]. Quantum chemical approaches to calculation of structures and optical spectra of metal clusters were reviewed in 1991 [64].

The remainder of this paper is organized as follows: background theory and photoabsorption cross-section and computational methods are described briefly; photoabsorption spectra from TDHF and BSE methods are presented and compared to CI calculations and/or experimental measurements; the accuracy of TDHF and BSE methods for small Na clusters is compared to CI methods and the failure of the TDA for these systems is discussed.

II. THEORY

A. BSE and TDHF methods

TDHF and BSE methods for calculating excited states in clusters and solids can be expressed as the generalized eigenvalue problem in Eq. (1). Both methods contain electron-hole attraction and hopping terms. The difference in the methods is that the electron-hole attraction term in BSE contains the screened Coulomb interaction whereas in TDHF it is unscreened. Furthermore, electron and hole energies (electron affinities and ionization potentials), in BSE in this work are dressed "quasiparticle" energies derived from G_oW_o calculations, whereas electron and hole energies are bare HF electron and hole energies in TDHF. Introduction of screening on going from TDHF to BSE methods results in two competing changes to TDHF excitation energies. Firstly, G_oW_o particle-hole gaps are typically reduced compared to HF gaps. This tends to reduce excitation energies. Secondly, screening of the electron-hole attraction results in an increase of excitation energies as the electron-hole attraction terms in the two-body hamiltonian strongly reduces the excitation energy. Since small Na clusters have few electrons and low-electron density, screening is weak in these finite systems so that TDHF and BSE methods yield quite similar results in many cases.

TABLE I. Table of matrix elements of A and B blocks of Eq. (1) for RPA, TDHF, and BSE approximations for a spin singlet molecule. Factors of two arise from summation over spin, tildes on energy eigenvalues for BSE indicate G_oW_o@HF eigenvalues and W_d is the dynamic part of the screened interaction W_o.

Method	Matrix elements
RPA A	$(\epsilon_a - \epsilon_i)\delta_{ij}\delta_{ab} + 2\,(ai\|jb)$
RPA B	$2\,(ai\|bj)$
TDHF A	$(\epsilon_a - \epsilon_i)\delta_{ij}\delta_{ab} + 2\,(ai\|jb) - (ab\|ji)$
TDHF B	$2\,(ai\|\|bj) - (ib\|ja)$
BSE A	$(\widetilde{\epsilon_a} - \widetilde{\epsilon_i}) + 2\,(ai\|bj) - (ab\|W_d\|ji)$
BSE B	$2\,(ai\|bj) - (ib\|W_d\|ja)$

$$\begin{pmatrix} A - \Omega & B \\ -B^* & -A^* - \Omega \end{pmatrix} \begin{pmatrix} X \\ Y \end{pmatrix} = 0. \tag{1}$$

The A and B matrices in Eq. (1) contain electron repulsion integrals (ERI) and HF or G_oW_o energy eigenvalues listed in Table I. Note that RPA in Table I refers to RPA excluding exchange and is equivalent to time-dependent Hartree (TDH) theory. The problem is usually expressed in a basis of single-particle eigenstates of the Fock or Kohn-Sham operator, whose occupied and virtual states are $\psi_i(\mathbf{r})$ and $\psi_a(\mathbf{r})$, respectively. Generalized eigenvectors which result from solution of Eq. (1) are linear combinations of products of eigenfunctions of the Fock operator, $X_{ai}^{\alpha}(\mathbf{r}) = c_{ai}^{\alpha}\psi_a(\mathbf{r})\psi_i^*(\mathbf{r})$ and $Y_{ai}^{\alpha} = d_{ai}^{\alpha}\psi_i(\mathbf{r})\psi_a^*(\mathbf{r})$.

Omission of the coupling B matrices in Eq. (1) is known as the Tamm-Dancoff approximation (TDA) [68,69]. It is commonly applied in solid-state BSE calculations in order to reduce computational cost. It is generally regarded as a good approximation, although this assumption has been tested to only a limited extent [38,43]. Its validity has been questioned recently for BSE calculations on organic systems [3,13].

B. G_oW_o approximation

The nonlocal self-energy operator Σ, which is used to calculate perturbative, G_oW_o corrections to HF energy eigenvalues in this work, is obtained from the convolution of the HF Green's function and the screened Coulomb interaction W_o given by

$$W_o(\mathbf{r}, \mathbf{r}', \epsilon) = v(\mathbf{r} - \mathbf{r}') + \int d\mathbf{r}'' d\mathbf{r}''' v(\mathbf{r} - \mathbf{r}'')\Pi^{\mathrm{RPA}} \times (\mathbf{r}'', \mathbf{r}'''; \epsilon) v(\mathbf{r}''' - \mathbf{r}'). \tag{2}$$

This form of the screened interaction is equivalent to the $\epsilon^{-1}v$ form commonly used in solid-state calculations, where ϵ^{-1} is the RPA inverse dielectric function and v is the bare Coulomb potential. The RPA polarizability Π^{RPA} in Eq. (2)

is obtained from a TDH calculation using the RPA A and B matrices (Table I). Calculation of W_o using Eqs. (2) and (3) is done without making any plasmon pole approximation, which is usually necessary when W_o is calculated from the RPA inverse dielectric function ϵ^{-1}. W_o expressed in a basis of eigenfunctions of the Fock operator becomes

$$W_{ai,bj} = (ai|bj) + \sum_{\alpha} w^{\alpha}_{ai} w^{\alpha}_{bj} \left(\frac{1}{\omega - \Omega^{\alpha} + i\eta} - \frac{1}{\omega + \Omega^{\alpha} - i\eta} \right), \quad (3)$$

where $(ai|bj)$ is an ERI in chemists' notation, superscript α denotes a particular generalized eigenvalue or eigenvector, η is a positive infinitesimal, introduced to ensure convergence of integrals in the complex plane which contain W_o as part of the integrand, and

$$w^{\alpha}_{ai} = (ai|ck)\left(X^{\alpha}_{ck} + Y^{\alpha}_{ck}\right). \quad (4)$$

The G_oW_o self-energy is given by

$$\Sigma(\mathbf{r}, \mathbf{r}'; \epsilon) = i \int_{-\infty}^{+\infty} d\epsilon' e^{i\epsilon'\eta} G_o(\mathbf{r}, \mathbf{r}'; \epsilon - \epsilon') W_o(\mathbf{r}, \mathbf{r}', \epsilon'). \quad (5)$$

When this is expressed in the basis of eigenfunctions of the Fock operator the diagonal elements of its matrix representation are

$$\Sigma_{kk}(\omega) = \sum_{\alpha,i,a} \left(\frac{w^{\alpha}_{ik} w^{\alpha}_{ki}}{\omega - \epsilon_i + \Omega^{\alpha} - i\eta} + \frac{w^{\alpha}_{ak} w^{\alpha}_{ka}}{\omega - \epsilon_a - \Omega^{\alpha} + i\eta} \right). \quad (6)$$

The static part of the self-energy, $(ai|bj)$, which arises from the first (bare Coulomb) term on the RHS of Eq. (2), is a HF exchange matrix element and is included in the Fock operator, which is diagonalized to yield HF eigenvalues. This term is not included in the HF self-energy to avoid double counting.

C. Photoabsorption cross-section

In SI units, the specific absorption coefficient in m^2 (per cluster valence electron) is

$$\sigma(E) = \sum_{\alpha} \frac{\hbar e^2}{\epsilon_0 m_e c} f_{\alpha} E \frac{\Gamma_{\alpha} E}{\left(E^2 - E^2_{\alpha}\right)^2 + (\Gamma_{\alpha} E)^2}. \quad (7)$$

where E and E_{α} are the photon and system excitation energies, Γ_{α} is the linewidth of an excitation (0.2 eV in this work), and f_{α} is the oscillator strength given by

$$f_{\alpha} = \frac{2}{3} \frac{m_e E_{\alpha} |x_{\alpha}|^2}{\hbar^2}, \quad (8)$$

where $-ex_{\alpha}$ is a transition dipole moment for an excitation and E_{α} is an excitation energy. According to the TRK sum rule, oscillator strengths for a particular system sum to the number of electrons, $\sum_{\alpha} f_{\alpha} = N$, available for excitation.

III. COMPUTATIONAL METHODS

HF, TDHF, GW, and BSE calculations reported in this work were performed using the Exciton code [13,70]. The HF module uses a conventional McMurchie-Davidson algorithm [71] for calculating four-center ERI and the GW and BSE modules use a resolution of the identity (RI) approach [72]. Full details of all methods used are given in Ref. [13].

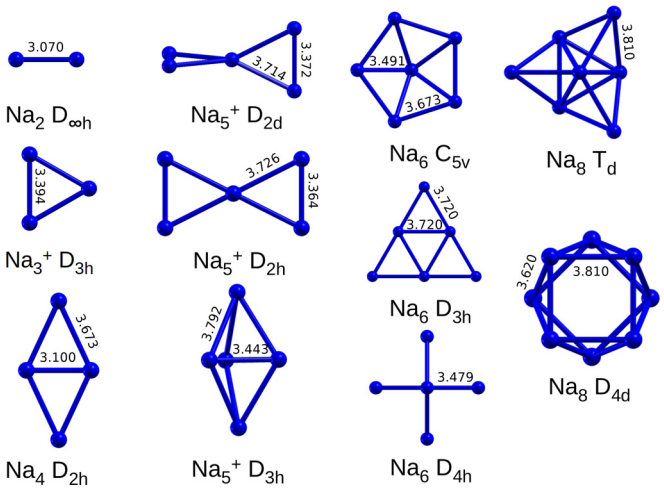

FIG. 1. Cluster structures and bond lengths in angstroms for Na_2 to Na_8 clusters used in this work. Note that the Na_6 D_{4h} cluster is a bicapped square and the distance between the capping atoms is 3.395 Å. Bond lengths in the inner tetrahedron of the Na_8 T_d cluster are 3.750 Å.

The wave function basis set used in all calculations reported here (and in Ref. [12]) is the $6-311{+}{+}G(3df, 3pd)$ Gaussian orbital basis, which includes diffuse and polarization functions [73] obtained from the EMSL database [74,75]. The auxillary basis set used to calculate three-center ERI in GW and BSE calculations is the cc-pVTZ-RI Gaussian basis by Weigend *et al.* [72].

All TDHF, G_oW_o, and BSE calculations excluded Na core states from the screened interaction and from the A and B matrices in Eq. (1). The cutoff in virtual states in each case was 1 Hartree, the same cutoff value was used by Priya *et al.* [12] in their FCI calculations.

Results for Na_2 from the TDHF-TDA module in Exciton were compared to results from the CIS module [76] in the GAMESS code [77,78] using the same Gaussian basis set. Excitation energies from either code differed by approximately 10 meV, which is reasonable since only the Exciton code uses the RI approximation for generation of ERI.

IV. RESULTS

The structures of clusters up to Na_8 whose photoabsorption cross-sections are reported here are shown in Fig. 1.

A. Na_2 and Na_3^+

TDHF, BSE, and FCI excitation energies and oscillator strengths for the three lowest $^1\Sigma_u^+$ and $^1\Pi_u$ states of Na_2 are given in Table II. For Na_2 to Na_5^+ equilibrium geometries were determined using the CCSD(T) coupled cluster method [12] and Na_6 geometries were determined using CCSD. The dimer bond length is 3.07 Å. The Na_3^+ trimer is an equilateral triangle with bond lengths of 3.39 Å [12]. Excitation energies and oscillator strengths for Na_2 are given in Table II.

TABLE II. Na_2 $D_{\infty d}$ excitation energies in eV and oscillator strengths. Columns labeled f contain oscillator strengths. Transition dipole moment orientations are given next to the state label. Blank entries indicate no data available.

State	TDHF	f	BSE	f	FCI[a]	f[a]
$1^1\Sigma_u^+$ z	2.00	0.63	2.13	0.63	1.87	0.62
$2^1\Sigma_u^+$ z	3.30	0.03	3.53	0.04	-	-
$3^1\Sigma_u^+$ z	4.26	0.01	4.44	0.01	-	-
$1^1\Pi_u$ (x, y)	2.42	1.11	2.67	1.22	2.48	1.28
$2^1\Pi_u$ (x, y)	3.44	0.16	3.62	0.12	3.66	0.24
$3^1\Pi_u$ (x, y)	4.95	0.07	5.00	0.09	4.62	0.05

[a]Reference [12].

Photoabsorption spectra generated using this data, the cross-section in Eq. (7) and a linewidth Γ of 0.2 eV are shown in Fig. 2. Oscillator strengths from TDHF, BSE, and FCI calculations are compared as black and red sticks in Fig. 2.

For Na_2 and Na_3^+, only excitation to the lowest state of each symmetry dominates the optical absorption spectrum. The $1^1\Sigma_u^+$ transition dominates transitions to $^1\Sigma_u^+$ states and occurs at 2.00, 2.13, and 1.87 eV in TDHF, BSE, and FCI calculations. Experiment [79] finds this transition at 1.82 eV. The $1^1\Pi_u$ transition in Na_2 occurs at 2.52 eV [80]. It dominates transitions to $^1\Pi_u$ states and occurs at 2.42, 2.67, and 2.48 eV according to TDHF, BSE and FCI methods (Table II). We adopt a labeling of states in order (1, 2, 3,...) for all clusters

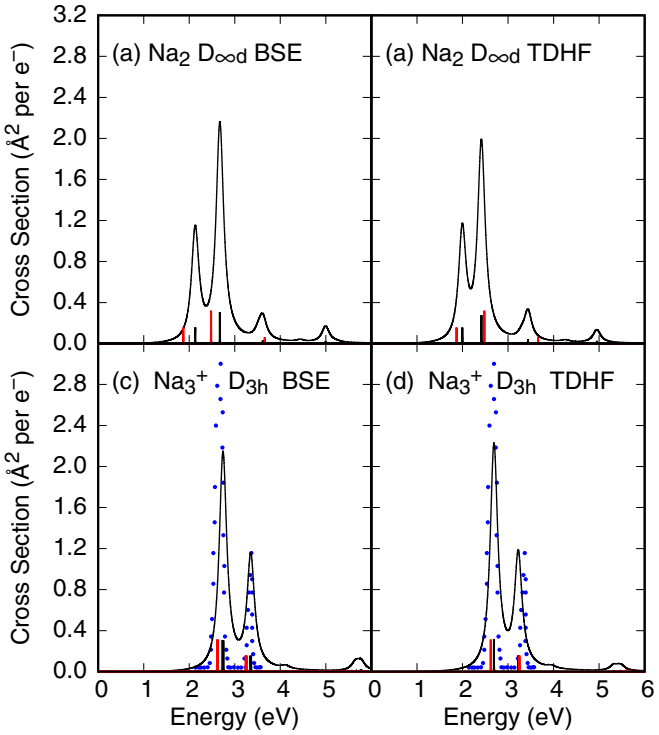

FIG. 2. BSE and TDHF photoabsorption cross-sections for Na_2 and Na_3^+. Oscillator strengths from BSE [(a) and (c)] and TDHF [(b) and (d)] calculations are shown as black sticks and those from FCI are shown in red. Blue dots in (c) and (d) are experimental data for Na_3^+ redrawn from Ref. [52].

TABLE III. Na_3^+ D_{3h} excitation energies in eV and oscillator strengths f.

State	TDHF	f	BSE	f	FCI[a]	f[a]
$1^1E'$ (x, y)	2.69	1.26	2.74	1.22	2.62	1.25
$2^1E'$ (x, y)	3.96	0.01	4.12	0.02	-	-
$3^1E'$ (x, y)	5.32	0.03	5.65	0.05	5.45	0.05
$4^1E'$ (x, y)	6.63	0.01	6.92	0.01	-	-
$1^1A_2''$ z	3.22	0.63	3.35	0.63	3.25	0.63
$2^1A_2''$ z	5.47	0.03	5.78	0.05	5.59	0.03
$3^1A_2''$ z	6.48	0.01	6.64	0.01	-	-

[a]Reference [12].

rather than the conventional (X, A, B, C,...) labeling of ground and excited states of diatomic species. For Na_6 and Na_{20} clusters, where strong optical excitations are not to lowest energy states, this label is omitted.

Comparison of oscillator strengths via stick diagrams in Figs. 2(a) and 2(b) shows that in both cases positions and oscillator strengths predicted by TDHF are in better agreement with FCI values than BSE with FCI. This might be expected as there are only two valence electrons and so the valence-valence interaction in Na_2 and Na_3^+ is unscreened (neglecting small core electron contributions). In this case, BSE overestimates transition energies $c.f.$ FCI, while TDHF underestimates it, contrary to expectation based on experience in solid-state HF and BSE calculations.

Excitations to the $1^1E'$ and $1^1A_2''$ states of Na_3^+ (Table III) possess the majority of oscillator strength parallel (x, y) and perpendicular (z) to the plane containing the cluster atoms. TDHF, BSE, and FCI predict excitation energies to the $1^1E'$ state of 2.69, 2.74, and 2.62 eV, respectively. The experimental excitation energy is 2.62 eV [52]. Oscillator strengths from these methods are in excellent agreement. There is also good agreement in predictions for excitations to the $1^1A_2''$ state, which is 3.33, 3.22, 3.35, and 3.25 eV according to experiment [52], TDHF, BSE, and FCI, respectively. Each method predicts the same oscillator strength, $f = 0.63$.

Summed oscillator strengths for Na_2 and Na_3^+ are given in Table IV. Only excitations from valence electron states are included. The basis set used yields an accurate expansion of valence states and numerical values of summed oscillator strengths are close to expected TRK values. What is perhaps surprising in Table IV is that summed oscillator strengths for TDHF-TDA and BSE-TDA approaches greatly exceed the number of valence electrons, N_{elec}, and that this violation of the TRK sum rule increases roughly linearly with the number of valence electrons (Fig. 3). Excitation energies, oscillator strengths and optical absorption spectra for BSE-TDA and TDHF-TDA approximations are compared to values from BSE and TDHF calculations in Ref. [81] (Fig. 1 and Tables I and II).

B. Na_4 and Na_5^+

The ground-state equilibrium geometry of Na_4 is a rhombus with D_{2h} symmetry and bond lengths of 3.10 and 3.67 Å [12]. The rhombus is oriented with the short bond length along the x direction and the long bond length along the y direction.

TABLE IV. Summed valence state oscillator strengths for TDHF and BSE calculations and their TDA approximations.

Species	N_{elec}	TDHF	TDHF-TDA	BSE	BSE-TDA
Na_2 $D_{\infty d}$	2	2.03	3.05	2.15	3.37
Na_3^+ D_{3h}	2	2.06	2.96	2.06	3.13
Na_4 D_{2h}	4	4.06	6.67	4.30	7.36
Na_5^+ D_{2d}	4	4.09	6.18	3.97	6.45
Na_5^+ D_{2h}	4	4.54	6.66	4.39	6.91
Na_5^+ D_{3h}	4	4.10	6.75	3.94	7.04
Na_6 C_{5v}	6	6.13	12.25	6.24	12.94
Na_6 D_{3h}	6	6.12	10.21	6.29	11.03
Na_6 D_{4h}	6	6.11	12.54	6.39	13.47
Na_8 T_d	8	8.16	16.58	8.37	17.66
Na_8 D_{4d}	8	8.18	21.04	8.12	21.79
Na_{20} C_s	20	20.32	66.66	18.67	67.00
Na_{20} C_3	20	20.32	63.74	18.72	64.14

Photoabsorption energies and oscillator strengths for the first three or four transitions of each dipole-active symmetry in TDHF and BSE calculations are compared to FCI and MRD-CI calculations in Table V. BSE and TDHF photoabsorption spectra are compared to the experimental spectrum of Na_4 redrawn from Ref. [53] and oscillator strengths are compared to FCI oscillator strengths as black (TDHF or BSE) and red (FCI) sticks in Fig. 4.

The experimental photoabsorption spectrum of Na_4 contains peaks at 1.8, 2.5, and 2.8 eV [53]. Each of the four theoretical methods predicts the strongest photoabsorption in transitions to $^1B_{2u}$, $^1B_{3u}$, and $^1B_{1u}$ excited states in agreement with these energies. The transition to the 1^1B_{2u} state is predicted at 1.93, 1.68, 1.71, and 1.74 eV by BSE, TDHF, FCI, and MRD-CI, respectively, and is assigned to the peak at 1.8 eV labeled B by Wang *et al.* [53]. The transition to the 2^1B_{3u} state is predicted at 2.58, 2.62, 2.47, and 2.52 eV and is assigned to the peak at 2.5 eV labeled E. FCI and MRD-CI predict the 1^1B_{1u} state at 2.09 and 2.12 eV, respectively, with a low photoabsorption cross-section and the strongest transition to the 2^1B_{1u} state at 2.70 and 2.80 eV, respectively. Peak F at 2.8 eV is assigned to this transition. For both BSE and TDHF methods, the strongest transition to a $^1B_{1u}$ state occurs for the 1^1B_{1u} state at 2.62 and 2.36 eV, respectively. The difference in distribution of oscillator strengths over the low-energy transitions of $^1B_{1u}$ symmetry can be seen in Table V.

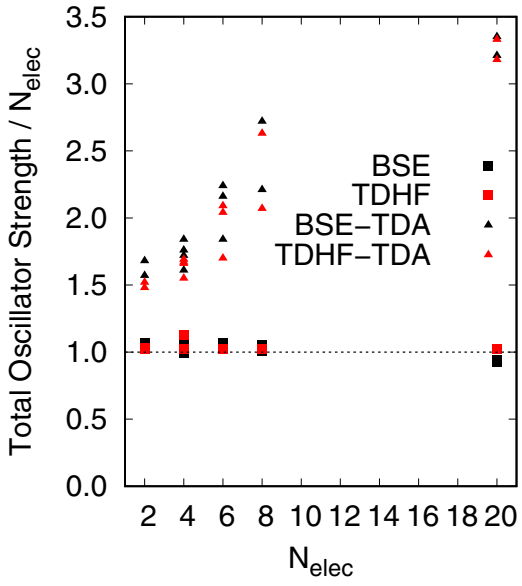

FIG. 3. Ratio of total oscillator strength to number of valence electrons for each cluster studied in this work. The Thomas-Reiche-Kuhn sum rule is satisfied on the horizontal dotted line where the total oscillator strength is equal to the number of valence electrons. Only valence electronic excitations are included in the total oscillator strength.

TABLE V. Na_4 D_{2h} excitation energies in eV and oscillator strengths f.

State	TDHF	f	BSE	f	FCI[a]	f[a]	MRD-CI[b]
1^1B_{3u} x	2.19	0.35	2.39	0.00	-	-	1.57
2^1B_{3u} x	2.62	0.62	2.58	1.03	2.47	0.77	2.52
3^1B_{3u} x	3.02	0.22	3.26	0.16	3.22	0.16	-
1^1B_{2u} y	1.68	1.00	1.93	1.10	1.71	1.15	1.74
2^1B_{2u} y	2.04	0.16	2.32	0.15	-	-	1.92
3^1B_{2u} y	2.54	0.05	2.80	0.03	-	-	-
1^1B_{1u} z	2.36	0.45	2.62	0.48	2.09	0.09	2.12
2^1B_{1u} z	3.07	0.17	3.10	0.37	2.70	0.62	2.80
3^1B_{1u} z	3.16	0.49	3.34	0.24	3.01	0.11	-
4^1B_{1u} z	4.32	0.08	4.22	0.08	3.28	0.14	-

[a]Reference [12].
[b]Reference [14].

The three lowest energy configurations of Na_5^+ investigated by Priya *et al.* [12] are a twisted bow-tie configuration with D_{2d} symmetry and bond lengths of 3.37 and 3.71 Å, a planar bow-tie configuration with D_{2h} symmetry and bond lengths of 3.36 and 3.73 Å and a trigonal bipyramid with D_{3h} symmetry and bond lengths of 3.44 and 3.79 Å (Fig. 1). The D_{2d} and D_{2h}

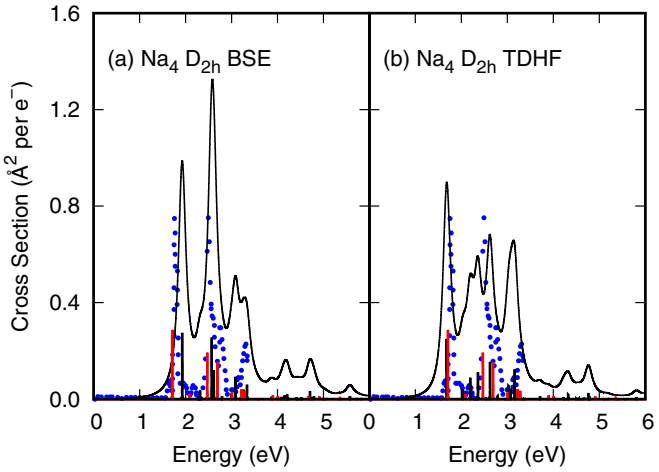

FIG. 4. BSE and TDHF photoabsorption cross-sections for Na_4 with D_{2h} point symmetry. Oscillator strengths from BSE (a) and TDHF (b) calculations are shown as black sticks and those from FCI are shown in red. Blue dots are experimental data for Na_4 redrawn from Ref. [53].

TABLE VI. Na_5^+ D_{2d} excitation energies in eV and oscillator strengths f.

State	TDHF	f	BSE	f	FCI[a]	f[a]
$1^1E\ (x, y)$	1.95	0.13	1.98	0.16	1.77	0.13
$2^1E\ (x, y)$	2.84	1.97	2.83	1.66	2.68	1.23
$3^1E\ (x, y)$	3.12	0.02	3.07	0.16	3.32	1.05
$4^1E\ (x, y)$	3.48	0.32	3.57	0.30	3.97	1.02
$1^1B_2\ z$	2.19	1.25	2.17	1.15	2.24	1.34

[a]Reference [12].

structures are almost isoenergetic after energy minimization using CCSD(T) [12]. The D_{3h} structure is 130 meV higher in energy [12].

Na_5^+ has three optical absorption peaks at 2.2, 2.8, and 3.3 eV [52]. These are well reproduced by FCI, BSE, and TDHF calculations for the two low-energy structures (D_{2d} and D_{2h}). In the D_{2d} cluster, strong photoabsorption occurs at 2.24, 2.68, and 3.32 eV in FCI, 2.17, 2.83, and 3.57 eV in BSE and 2.19, 2.84, and 3.48 eV in TDHF (Table VI), all in agreement with experiment. The first of these excited states is the 1^1B_2 state with its transition dipole moment along the (long) z axis of the cluster. The second is the 2^1E state and the third is the 3^1E state. The transition to the 1^1E state occurs at 1.77 eV in FCI but has a relatively low oscillator strength, in all three methods ($f = 0.13$ in FCI). While there is good agreement between the three methods in excitation energies of the first four ^1E states, there is some variation in oscillator strength, especially in the 3^1E state (Table VI).

There is also good agreement between experiment, FCI, BSE, and TDHF in positions of the main photoabsorption peaks for the D_{2h} structure. Here the two short bond lengths lie along the x axis, the long cluster axis is y and z is perpendicular to the plane. Oscillator strength is distributed over three symmetries and there is better agreement than in the D_{2d} cluster (Table VII). The peaks occur at 2.15, 2.16, and 2.19 eV in FCI, BSE and TDHF (1^1B_{2u} excited state), 2.51, 2.51, and 2.54 eV (1^1B_{3u} excited state) and 3.22, 3.22, and 3.13 eV (1^1B_{1u} excited state). Here all three methods predict three photoabsorption features of roughly equal intensity, as found in experiment [52].

Agreement between theory and experiment in the less stable D_{3h} structure is not as good. Each method predicts two strong photoabsorption peaks instead of the three found in experiment (Fig. 5). Oscillator strengths and excitation energies for the D_{3h} structure are given in Table III in Ref. [53].

TABLE VII. Na_5^+ D_{2h} excitation energies in eV and oscillator strengths f.

State	TDHF	f	BSE	f	FCI[a]	f[a]
$1^1B_{1u}\ z$	3.13	1.11	3.22	1.13	3.22	1.13
$1^1B_{2u}\ y$	2.19	1.26	2.16	1.15	2.15	1.35
$1^1B_{3u}\ x$	2.54	1.03	2.51	1.05	2.51	1.13
$2^1B_{3u}\ x$	2.89	0.20	2.76	0.06	3.62	0.08

[a]Reference [12].

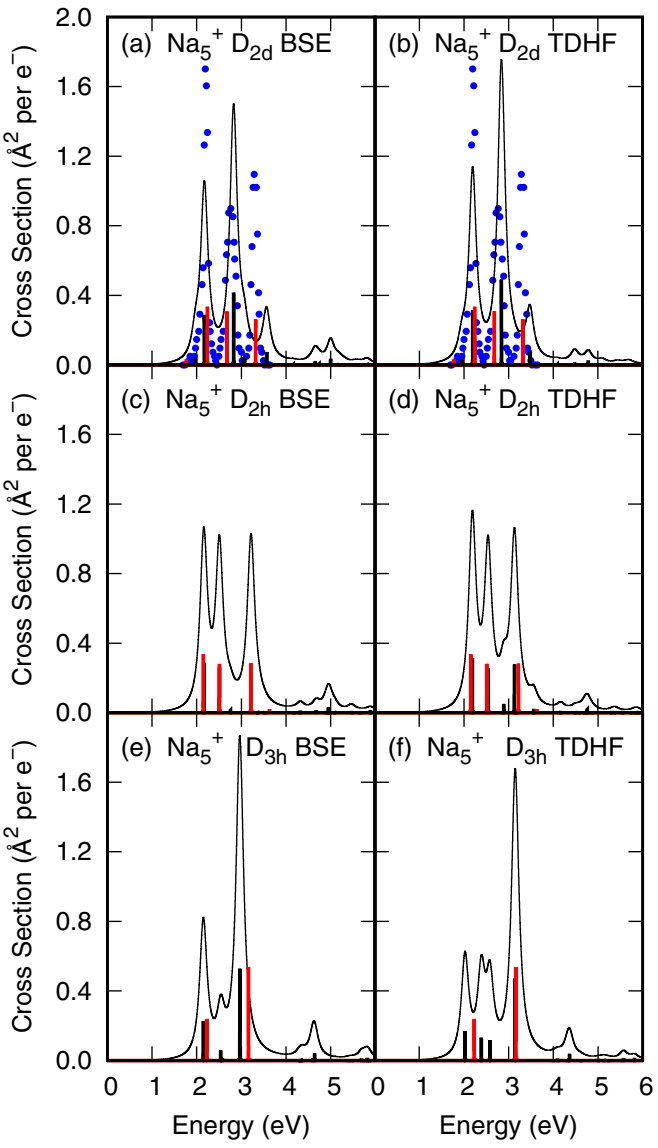

FIG. 5. BSE and TDHF photoabsorption cross-sections for Na_5^+ with D_{2d}, D_{2h}, and D_{3h} point symmetries. Oscillator strengths from BSE [(a), (c), and (e)] and TDHF [(b), (d), and (f)] calculations are shown as black sticks and those from FCI are shown in red. Blue dots in (a) and (b) are experimental data for Na_5^+ redrawn from Ref. [52].

C. Na_6

The lowest energy structures of Na_6 are a capped pentagon with C_{5v} symmetry, a planar structure with D_{3h} symmetry and a bicapped square structure with D_{4h} symmetry (Fig. 1). The C_{5v} structure is the ground state and the D_{3h} and D_{4h} structures are 90 and 185 meV higher in energy, respectively, in a CCSD geometry optimization [12]. CI calculations by Priya *et al.* [12] for Na_6 clusters were restricted to excitations up to quadruples, denoted here as QCI.

There are three main features in the Na_6 C_{5v} QCI photoabsorption calculation at 2.15, 2.53, and 2.79 eV, which can be compared to 2.12, 2.74, and 2.89 eV in BSE and 2.09, 2.58, and 3.00 eV in TDHF [Figs. 6(a) and 6(b), Table VIII]. Both BSE and TDHF reproduce the QCI main peak at 2.15 eV well. Experimental photoabsorption peaks are found at 1.78,

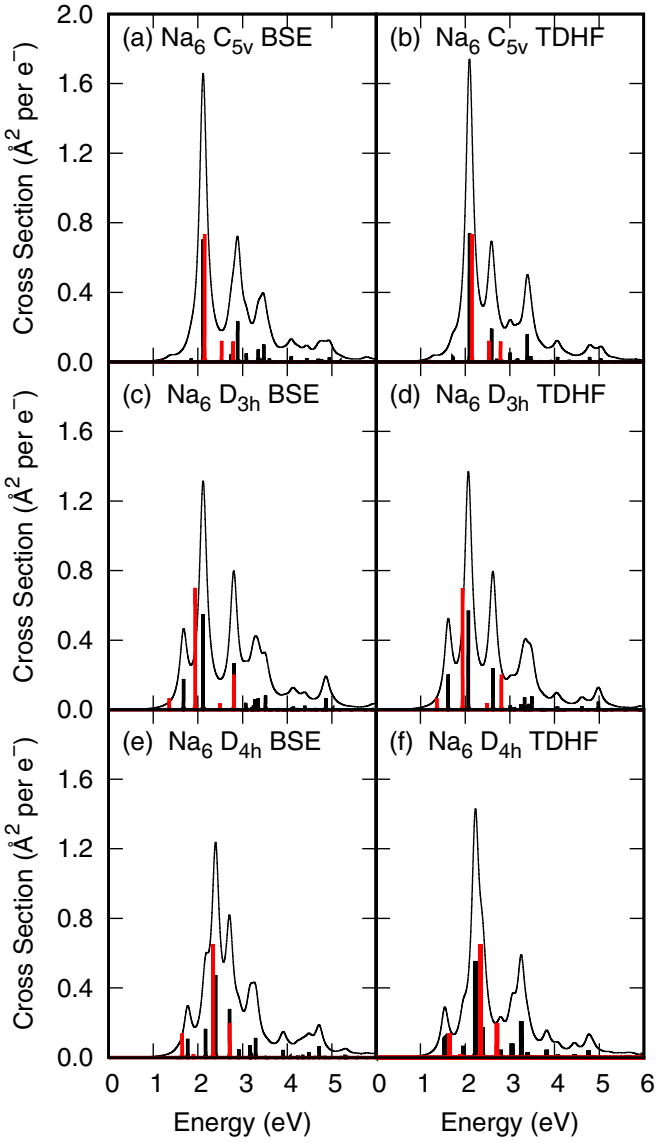

FIG. 6. BSE and TDHF photoabsorption cross-sections for Na_6 with C_{5v}, D_{3h}, and D_{4h} point symmetries. Oscillator strengths from BSE [(a), (c), and (e)] and TDHF [(b), (d), and (f)] calculations are shown as black sticks and those from FCI are shown in red.

2.08, 2.44, and 2.83 eV [82]. The excitations to $^1E_1$ states with low photoabsorption cross-sections at 1.72 eV in TDHF and at 1.85 eV in BSE may correspond to the experimentally observed absorption at 1.78 eV.

There are four main optically active excitations in the QCI optical spectrum of the D_{3h} structure at 1.36, 1.94, and 2.49 eV ($^1E'$ excited state) and at 2.71 eV ($^1A_2''$ excited state). The BSE calculation for the D_{3h} structure has corresponding absorptions at 1.68, 2.12 and 2.80 eV ($^1E'$) and at 2.80 eV ($^1A_2''$) and the TDHF calculation at 1.62, 2.07, and 2.62 eV ($^1E'$) and 2.62 eV ($^1A_2''$). Photoabsorption spectra are shown in Figs. 6(c) and 6(d) and excitation energies and oscillator strengths are given in Table IV in Ref. [81].

There are three main features in the QCI photoabsorption spectrum of the D_{4h} structure at 1.65 and 2.34 (^1E_u excited state) and at 2.71 eV ($^1A_{2u}$ exited state). The BSE calculation has corresponding peaks at 1.77 and 2.40 eV (^1E_u excited state) and 2.71 eV ($^1A_{2u}$ excited state) and the TDHF calculation has peaks at 1.54 and 2.23 eV (^1E_u excited state) and at 2.39 and 3.26 eV ($^1A_{2u}$ excited state). Photoabsorption spectra are shown in Figs. 6(e) and 6(f) and excitation energies and oscillator strengths are given in Table V in Ref. [81].

TABLE VIII. Na_6 C_{5v} excitation energies in eV and oscillator strengths f.

State	TDHF	f	BSE	f	QCI[a]	f[a]
$^1E_1$ (x, y)	1.72	0.11	1.85	0.08	-	-
$^1E_1$ (x, y)	2.09	2.95	2.12	2.83	2.15	2.95
$^1E_1$ (x, y)	2.58	0.24	2.74	0.17	2.53	0.48
$^1E_1$ (x, y)	3.00	0.22	3.35	0.28	-	-
$^1A_1$ z	2.59	0.76	2.77	0.16	2.79	0.47
$^1A_1$ z	3.39	0.63	2.89	0.93	-	-
$^1A_1$ z	3.47	0.13	3.47	0.40	-	-

[a]Reference [12].

D. Na_8

Na_8 is more abundant than neighboring Na_7 or Na_9 clusters by a factor or two or three in cluster beam studies [46], indicating relatively high stability; it is an Na_n magic number cluster. There are several low-energy structures, including a D_{2d} symmetry cluster [14,57,59], a square antiprism with D_{4d} symmetry [14,59] and a tetra-capped Na_4 tetrahedron with T_d symmetry, which is the HF ground-state structure [14,59]. The T_d and D_{4d} structures are considered here and the bond lengths given in Ref. [14] are used. Multireference singles and doubles CI (MRD-CI) [14] calculations are available for the T_d and D_{4d} structures and RPA (TDHF) calculations are available for the T_d structure [83]. According to Ref. [14], the CI energy for the D_{4d} structure is 76 meV higher in energy than the T_d structure. Furthermore, a TDLDA calculation is available for spherical jellium Na_8 [29].

Energies of the first five photoabsorption peaks in T_d Na_8 from two TDHF calculations, a BSE calculation and MRD-CI are given in Table IX. The TDHF calculation by Gatti *et al.* [83] and the MRD-CI calculation used Na effective core potentials and the basis set contained three s and two p Gaussian functions per Na atom. This work used an all electron Na basis set where the valence part contained five s, five p, three d, and one f valence basis functions per atom. It is not surprising,

TABLE IX. Na_8 T_d excitation energies in eV and oscillator strengths f.

State	TDHF[a]	f	TDHF[b]	f	BSE[a]	f	MRD-CI[c]	f
1^1T_2	1.61	0.66	1.71	0.62	1.69	0.34	1.59	0.45
2^1T_2	1.89	0.64	2.01	0.53	1.91	1.28	1.79	0.14
3^1T_2	2.31	3.00	2.48	2.84	2.43	2.92	2.09	0.60
4^1T_2	2.61	1.46	2.81	1.65	2.74	0.64	2.51	2.82
5^1T_2	3.00	0.18	3.16	0.06	3.01	0.25	2.60	0.27

[a]This work.
[b]Reference [83].
[c]Reference [14].

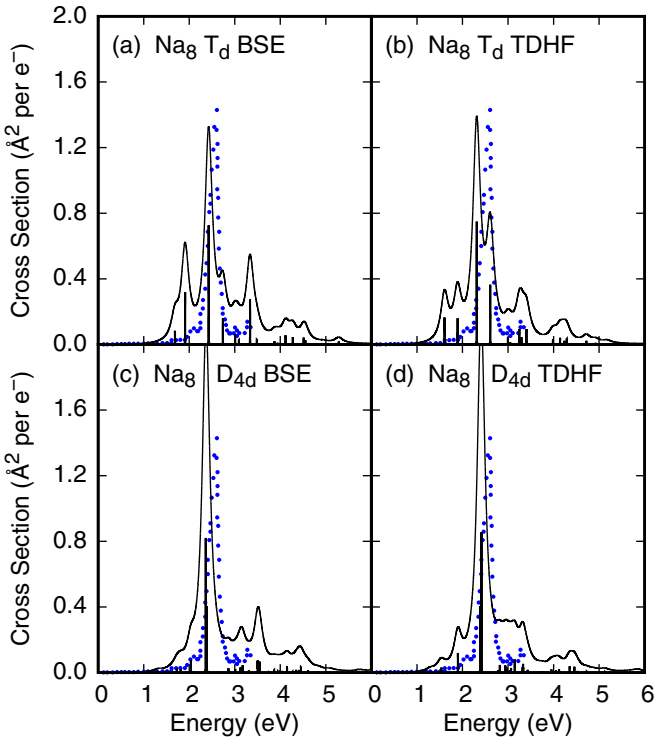

FIG. 7. BSE and TDHF photoabsorption cross-sections for Na_8 with T_d and D_{4d} point symmetries. Oscillator strengths from BSE [(a) and (c)] and TDHF [(b) and (d)] calculations are shown as black sticks. Blue dots are experimental data for Na_8 redrawn from Ref. [53].

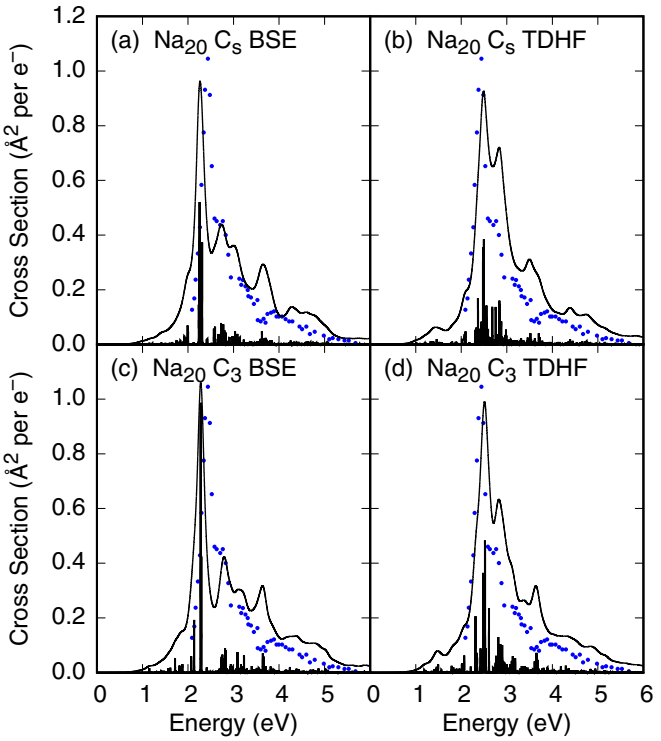

FIG. 8. BSE and TDHF photoabsorption cross-sections for Na_{20} with C_s or C_3 point symmetries. Oscillator strengths from BSE [(a) and (c)] and TDHF [(b) and (d)] calculations are shown as black sticks. Blue dots are experimental data for Na_{20} redrawn from Ref. [85].

therefore to see that the TDHF excitation energies predicted in this work lie 0.1 to 0.2 eV below those predicted by Gatti *et al.* The distribution of oscillator strength among these excitations is similar, with the maximum photoabsorption cross-section in excitation to the 3^1T_2 state. BSE excitation energies are up to 0.1 eV higher than the TDHF calculation in this work and MRD-CI excitation energies are systematically lower in energy. Photoabsorption spectra from the BSE and TDHF calculations from this work are compared to the experimental spectrum in Figs. 7(a) and 7(b).

The experimental spectrum is dominated by absorption at 2.6 eV with weaker absorptions on either side. Oscillator strengths from each of the four methods show one dominant photoabsorption. For the two TDHF calculations and the BSE calculation this is excitation to the 3^1T_2 state ($f = 3.00$, 2.84 and 2.92, Table IX) and for the MRD-CI calculation this is excitation to the 4^1T_2 state ($f = 2.82$). The corresponding excitation energies are 2.31, 2.48, 2.43, and 2.51 eV, in reasonable agreement with the 2.6 eV experimental value.

The photoabsorption spectrum for the D_{4d} square antiprism is also dominated by one excitation to a state of $^1E_1$ symmetry. Photoabsorption spectra from the BSE and TDHF calculations from this work are compared to the experimental spectrum in Figs. 7(c) and 7(d). The TDHF, BSE, and MRD-CI excitation energies for this transition are 2.42, 2.36, and 2.70 eV, which compares to the experimental excitation energy of 2.6 eV. Additional excitation energies and oscillator stengths for the D_{4d} structure are given in Table VI in Ref. [81].

E. Na_{20}

Na_{20} is known to be a magic number cluster from its relative abundance [46] and low specific polarizability [47] in cluster beam experiments. Its electronic configuration is expected to be stable as it has a $1s^21p^61d^{10}2s^2$ closed shell electronic configuration. Its photoabsorption spectrum consists of two strong peaks at 2.4 and 2.7 eV [54,84,85] and additional spectral weight with possible peaks at 3.2 and 4.0 eV, the highest of which has been assigned to a volume plasmon [85]. Several RPA (TDHF) calculations for Na_{20} have been reported using jellium spheres [17,27,29,30] or *ab initio* methods where the atomic structure adopted was a relaxed fcc lattice fragment [86] or TDLDA calculations which adopted icosahedral and trigonal bipyramidal structures [26]. Studies of the structure of Na_{20} using DFT molecular dynamics [67,87] or an empirical potential [88] followed by DFT optimization found a ground-state structure with C_s point symmetry. However, a recent study [66] using a particle swarm optimization method found a Na_{20} structure with C_3 point symmetry which was lower in energy than the C_s structure by 60 meV (Møller-Plesset MP2 theory) or 150 meV using a CCSD method.

Spherical jellium RPA calculations for the photoabsorption spectrum of Na_{20} by Yannouleas and coworkers [29] found two strong peaks at 2.6 and 2.9 eV with roughly equal oscillator strength and oscillator strength distributed over many modes up to 5 eV. Guet and Johnson [30] using a similar approach found similar optical absorption at 2.5 and 2.8 eV.

TABLE X. Na_{20} C_s excitation energies in eV and oscillator strengths f.

State	TDHF[a]	f	BSE[a]	f	Expt.[b]	f
$^1A'$ (x, y)	2.30	0.21	1.99	0.28	-	-
$^1A'$ (x, y)	2.33	0.25	2.24	0.53	-	-
$^1A'$ (x, y)	2.39	0.23	-	-	-	-
$^1A'$ (x, y)	2.48	1.41	-	-	-	-
$^1A'$ (x, y)	2.49	1.54	2.25	2.08	2.42	0.40
$^1A'$ (x, y)	2.55	0.57	2.31	1.50	-	-
$^1A'$ (x, y)	2.59	0.22	-	-	-	-
$^1A'$ (x, y)	2.84	0.60	2.78	0.27	2.77	0.10
$^1A'$ (x, y)	2.84	0.55	2.80	0.21	-	-
$^1A'$ (x, y)	2.88	0.33	-	-	-	-
$^1A'$ (x, y)	2.99	0.13	3.03	0.19	3.17	0.13
$^1A'$ (x, y)	-	-	-	-	4.04	0.15
$^1A''$ z	2.37	0.68	2.24	1.16	2.42	0.40
$^1A''$ z	2.44	0.33	2.29	0.31	-	-
$^1A''$ z	2.46	0.22	2.57	0.23	-	-
$^1A''$ z	-	-	2.59	0.26	-	-
$^1A''$ z	2.68	0.55	2.73	0.25	2.77	0.10
$^1A''$ z	2.76	0.54	-	-	-	-
$^1A''$ z	2.86	0.27	-	-	-	-
$^1A''$ z	2.98	0.22	3.09	0.13	3.17	0.13
$^1A''$ z	-	-	-	-	4.04	0.15

[a]This work.
[b]Reference [85].

TABLE XI. Na_{20} C_3 excitation energies in eV and oscillator strengths f.

State	TDHF[a]	f	BSE[a]	f	Expt.[b]	f
E (x, y)	2.06	0.25	1.72	0.21	-	-
E (x, y)	2.31	0.77	1.88	0.12	-	-
E (x, y)	2.34	0.29	-	-	-	-
E (x, y)	2.42	0.35	-	-	-	-
E (x, y)	2.48	1.46	2.28	3.94	2.42	0.40
E (x, y)	2.52	0.60	-	-	-	-
E (x, y)	2.54	0.35	-	-	-	-
E (x, y)	2.61	0.94	2.76	0.25	-	-
E (x, y)	2.76	0.24	2.77	0.15	2.77	0.10
E (x, y)	2.81	0.50	2.79	0.20	-	-
E (x, y)	2.90	0.40	2.82	0.35	-	-
E (x, y)	3.13	0.23	3.08	0.14	-	-
E (x, y)	3.18	0.21	3.09	0.29	3.17	0.13
E (x, y)	3.65	0.29	3.64	0.26	-	-
E (x, y)	3.68	0.18	3.66	0.21	-	-
^1A z	2.35	0.22	2.14	0.77	-	-
^1A z	2.45	0.14	-	-	-	-
^1A z	2.52	1.84	2.29	1.68	2.42	0.40
^1A z	2.81	0.30	2.74	0.15	-	-
^1A z	2.83	0.22	2.83	0.22	2.77	0.10
^1A z	-	-	2.86	0.42	-	-
^1A z	-	-	2.95	0.14	-	-
^1A z	-	-	3.11	0.15	-	-
^1A z	3.66	0.12	3.61	0.16	-	-

[a]This work.
[b]Reference [85].

Bonačić-Koutecký and coworkers [86] used an *ab initio* RPA approach and a relaxed fcc tetrahedral structure and found optical absorption at 2.2, 2.4, and 2.8 eV and a spectral density quite different from the spherical jellium results. Here we report TDHF and BSE calculations for Na_{20} clusters with C_s or C_3 symmetry using coordinates from Ref. [66].

The shell structure of occupied and virtual levels in a spherical jellium structure is $1s^2 1p^6 1d^{10} 2s^2 1f^0 2p^0 2d^0$. The shell structure is evident from a density of states plot for Na_{20} C_3 in Fig. 2 of Ref. [81]. The occupied levels clearly split into an *spds* structure. The lowest virtual states are bound by tens of meV or are unbound. The lowest virtual states are *1f* in character and are followed by *2d* levels which have a Rydberg character. The gap between occupied and virtual levels at the HF level is 3.4 eV. Ten occupied and 500 virtual levels were included in the TDHF and BSE calculations leading to a state space of 5000 optical transitions. Photoabsorption spectra for C_s and C_3 structures are compared to experimental data from Ref. [85] in Fig. 8.

Oscillator strengths for the strongest optical transitions in BSE and TDHF calculations on the C_s symmetry cluster are given in Table X and corresponding data for the C_3 symmetry cluster are given in Table XI. These are compared to spectral weights in eV $Å^2$ under three curves fitted to the experimental optical absorption spectrum in Ref. [85]. The authors of Ref. [85] note that the experimentally measured oscillator strength corresponds to 70% of the TRK sum rule theoretical value and this is consistent with comparison of experimental data and the calculated optical spectra in Fig. 8. Tables X and XI show that for excitations with the transition dipole moment polarized along the z axis ($^1A''$ or ^1A symmetry) and in the (x, y) plane ($^1A'$ or ^1E symmetry), there are series of relatively strong transitions in the range 2 to 3 eV, peaking at 2.48 eV (x, y) and 2.52 eV (z) in TDHF calculations and at 2.28 eV (x, y) and at 2.29 eV (z) in BSE calculations on the C_s symmetry cluster. Moving to the C_3 symmetry cluster, the strongest transitions occur at 2.49 eV (x, y) and at 2.37 eV (z) in TDHF calculations and at 2.25 eV (x, y) and at 2.24 eV (z).

Lorentzian lineshape peaks fitted to experimental data [85] found the strongest peak at 2.42 eV, which compares well with the strongest optical transitions in TDHF and BSE calculations noted above. TDHF calculations overestimate the fitted peak position by less than 0.1 eV and BSE calculations underestimate it by up to 0.2 eV. Comparison of the predicted optical absorption lineshapes in Fig. 8 shows good agreement between experiment and especially the BSE calculations for the C_s and C_3 symmetry clusters. Lineshapes fitting to experimental data in Ref. [85] also found peaks at 2.77, 3.17, and 4.04 eV, with areas of 25% to 30% of the main peak at 2.42 eV. Although the BSE calculations underestimate the main peak position by up to 0.2 eV, the relative intensity of the main peak and the spectral weight in the range 2 to 4 eV is better than for TDHF calculations.

Both theoretical methods show photoabsorption around 3.6 eV which is not found in experimemt. There are interesting differences in oscillator strength distribution which depend on method, but not cluster structure. The main peak in the BSE calculations contains only one or two modes which

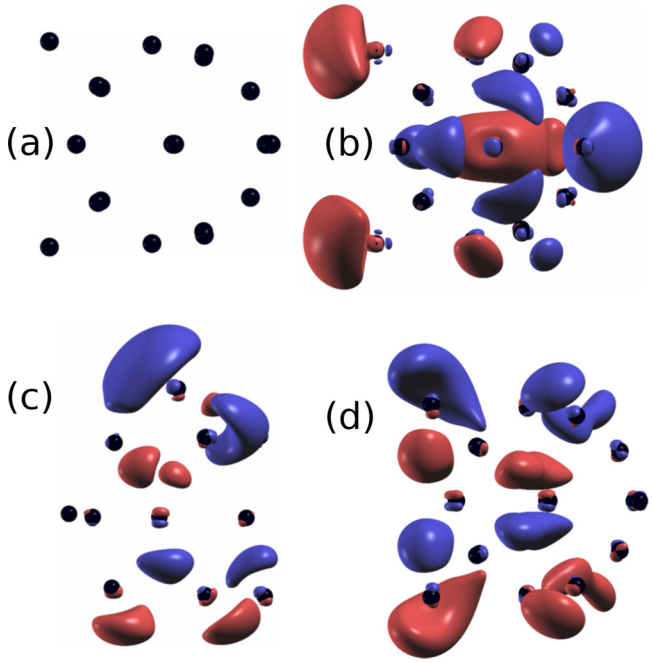

FIG. 9. Na_{20} C_s cluster structure and isosurfaces of BSE transition charge densities in the main optical absorption peak. (a) Cluster structure. (b) Mode at 2.31 eV with x polarization. (c) Mode at 2.25 eV with y polarization. (d) Mode at 2.24 eV with z polarization. (a), (b), and (d) are viewed in the xz plane and (c) is viewed in the xy plane, which is the symmetry mirror plane.

capture almost all the oscillator strength within 0.5 eV on either side of the peak, while the TDHF calculations show a broader distribution of oscillator strength instead. The tendency to gather oscillator strength into one or a few modes is characteristic of a collective excitation. The TDHF lineshape contains two peaks at 2.5 and 2.8 eV, in agreement with previous jellium calculations [29,30], although the oscillator strength is not simply distributed in two dominant peaks as it is in the jellium calculations. This may be due to the breaking of spherical symmetry in clusters with atomic structure, yet retaining the general tendency to have oscillator strength distrubuted as though there are only two dipole active modes.

The authors of Ref. [85] interpret a broad feature in the optical absorption spectrum centered at 4.04 eV as a volume plasmon with a large linewidth of 1.19 eV. This is not consistent with the TDHF and BSE oscillator stengths and transition charge densities in this work. The broad feature is reproduced in calculations in the range 4 to 5 eV (Fig. 8) but is due to a large density of modes with low oscillator strength, rather than an additional collective mode with a volume plasmon character.

Transition charge density isosurfaces for the strongest modes contributing to the main optical absorption peak in the C_s cluster from a BSE calculation are shown in Fig. 9. Each mode consists of polarization charge with a binodal structure along one Cartesian axis. Hence the modes are neither surface modes (with charge polarization in shells on surface atoms) nor volume modes (with a single nodal plane and most charge polarization in the cluster center). It is likely that the transition to a more bulklike optical response with distinct surface and volume modes occurs at much larger cluster sizes since Na_{20} consists only of two "bulk" atoms and 18 surface atoms.

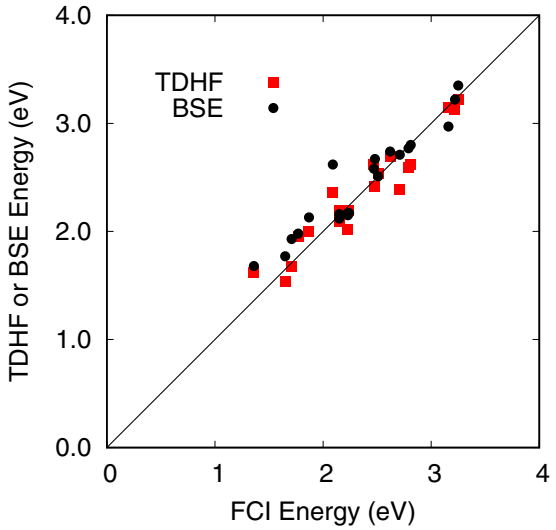

FIG. 10. Lowest dipole active excitation energies of each symmetry in nine Na clusters with two, four or six valence electrons compared to corresponding FCI excitation energies.

V. DISCUSSION

In this section, the agreement of TDHF and BSE results with FCI results is assessed and the origin of the failure of TDA approximations to TDHF or BSE calculations is discussed.

In all, nine clusters with between two and six Na atoms were studied for which direct comparisons with FCI calculations [12] are possible. Mean absolute differences (MAD) in excitation energy were calculated using the lowest TDHF or BSE excitation energy of each dipole active symmetry and the corresponding FCI energies. For TDHF, the MAD energy is 0.12 eV with largest deviations from the FCI excitation energy of +0.27 eV for the lowest $^1B_{1u}$ state of Na_4 and +0.26 eV for the lowest $^1E'$ state of D_{3h} Na_6. For BSE, the MAD enery is also 0.12 eV with largest deviations from FCI excitation energy of +0.53 eV for the lowest $^1B_{1u}$ state of Na_4 and +0.32 eV for the lowest E' state of D_{3h} Na_6. A plot of lowest TDHF and BSE excitation energies of each dipole active symmetry versus FCI excitation energies in each of the nine clusters is shown in Fig. 10. Data points are tightly clustered around the line where there is agreement with FCI results, except for the outliers mentioned above.

Introduction of screening on going from a TDHF to a BSE calculation introduces shifts in excitation energies of molecules which counteract each other (see Supporting Information in Ref. [13]). A perturbative G_oW_o calculation of the self-energy reduces single-particle excitation energies ($\widetilde{\epsilon_a} - \widetilde{\epsilon_i}$) below differences in HF Fock matrix eigenvalues ($\epsilon_a - \epsilon_i$, Table I) and therefore *lowers* transition energies in a G_oW_o/BSE calculation while introduction of screening of the electron-hole interaction on going from a TDHF to a BSE calculation reduces the strength of the electron-hole attraction and hence *raises* the transition energy. Depending

on which of these effects is greater, BSE excitation energies may be greater or smaller than TDHF excitation energies. For the Na_2 and Na_3^+ two electron systems, BSE predicts higher excitation energies than TDHF and TDHF excitation energies are in better agreement with FCI values. The average overestimate by BSE of the two lowest excitation energies for these systems is 0.17 eV while for TDHF it is 0.03 eV. The electron-electron interaction in these two valence electrons is essentially unscreened (if small core electron contributions are neglected) and so TDHF, which does not contain a screened interaction, is expected to yield better agreement with FCI energies.

Previous *GW*/BSE studies of Na clusters used a Kohn-Sham local density approximation (LDA) starting point. References [31] and [34] reported LDA HOMO-LUMO gaps of 0.55 and 0.58 eV, respectively, for Na_4. The LDA gap in Ref. [34] increased to 3.24 eV at the G_oW_o level and changed only marginally to 3.23 eV when a degree of self-consistency was included in the *GW* calculation. A HF starting point for these systems yields single particle HOMO and LUMO separations much closer to G_oW_o and self-consistent *GW* separations. In this work, the HF HOMO-LUMO gap for Na_4 is 3.74 eV. It increases slightly to 3.75 eV at the G_oW_o level with downward self-energy shifts of -0.40 and -0.39 eV for the HOMO and LUMO levels. Further evidence for weak screening in small Na clusters comes from similarly good prediction of FCI excitation energies by both TDHF (where the electron-hole interaction is unscreened and bare electron and hole energies are used) and BSE (where the electron-hole interaction is screened and dressed quasiparticle electron and hole energies are used). Onida *et al.* calculated the effective screening of a positive test charge placed at the center of an Na_4 cluster [31]. They found that the effective screening of the test charge potential was 1.2 at a distance of 5 bohr, whereas it would have been around 50 at that distance in bulk Na.

Photoabsorption spectra obtained for Na_4 beginning from an LDA calculation agree well with experiment, although the authors found an absorption threshold around 1.3 eV [32], which is absent from experiment and TDHF, BSE, or FCI calculations. BSE calculations on closed shell Na_2 to Na_8 clusters by Pal *et al.*, including positively charged clusters with odd numbers of Na atoms, are in good agreement with BSE calculations reported here. They used an effective core potential approach, a smaller basis set and equilibrium cluster geometries differ from those used here.

The Tamm-Dancoff approximation (TDA) to the Bethe-Salpeter equation (BSE-TDA) is generally acknowledged to provide excitation energies and photoabsorption cross-sections for periodic systems without strong electron-electron correlations in good agreement with experiment [38]. BSE-TDA calculations have been shown to yield results in reasonable agreement with experiment for a wide range of organic molecules [1,2,9,13]. However, in this work, it is found that both BSE-TDA and TDHF-TDA approximations yield photoabsorption spectra which differ from corresponding BSE and TDHF calculations in photoabsorption cross-section (see in Ref. [81] Fig. 1 and Tables I and II). BSE and TDHF methods are conserving approximations, in the sense of Baym and Kadanoff [42] and photoabsorption spectra computed using these approximations are expected to satisfy the TRK sum rule. It has been noted previously [89] that the CI singles (CIS) method, which is equivalent to the TDHF-TDA approximation, does not satisfy the TRK sum rule. Figure 3 and Table IV show that both TDHF and BSE numerical approaches in this work yield total oscillator strengths in good agreement with TRK values (the number of valence electrons N_{elec}). TDHF calculations presented here typically yield agreement with the TRK value to 2% with a MAD of 3% and a worst overestimate of 13%. BSE calculations have a MAD of 5% and a worst overestimate of 10%.

The correspondence between two coupled cluster doubles (CCD) approaches and TDHF and TDHF-TDA approaches has been discussed by Scuseria *et al.* [90]. They showed that CCD equations, where a certain set of diagrams is retained (which they denote as ring CCD), can be exactly rearranged as the TDHF equations [Eq. (1)] and given by

$$B = AT + TA + TBT = 0, \tag{9}$$

where A and B matrices are the TDHF A and B matrices. T is a CCD double excitation amplitude related to the TDHF X and Y eigenvector matrices by $T = YX^{-1}$ or $Y = TX$ and so $X + Y = (1 + T)X$. T is negative definite [90]. The transition dipole moment in a TDHF or BSE calculation depends on the amplitude $(X + Y)$. Setting the B matrix to zero in Eq. (1) means that Y is zero. Assuming that X does not change on going from a TDHF to a TDHF-TDA calculation and given that T is negative definite, it can be expected that a TDHF-TDA or BSE-TDA calculation will overestimate oscillator strengths.

Free and nearly-free electron metals are not usually regarded as strongly correlated electron systems (with large T amplitudes). Typical strongly correlated systems include doped transition metal oxide systems where there are holes in the transition metal d band. Nevertheless, generalized valence bond (GVB) calculations on Li clusters [91] show that electrons in alkali metal clusters are localized individually in atomic interstices. T (and Y) amplitudes in Na clusters can be expected to be large since strong intra-pair correlations are generated by double excitations from the HF determinant, illustrated by the calculations of McAdon and Goddard on Li clusters [91]. If T amplitudes are large and negative, and dipole transition amplitudes $X + Y$ depend on T as $(1 + T)X$, then the TDA can be expected to overestimate photoabsorption oscillator strengths to a significant extent.

VI. SUMMARY AND CONCLUSIONS

TDHF and BSE calculations for a series of closed shell calculations (Na_2, Na_3^+, Na_4, Na_5^+, Na_6, Na_8, and Na_{20}) have been presented. Detailed comparisons have been made between predicted optical absorption spectra from these methods and FCI (Na_2, Na_3^+, Na_4, Na_5^+) and QCI (Na_6) calculations using the same, extensive all electron Gaussian orbital basis set. The MAD in a series of 20 excited states for both TDHF and BSE calculations is 0.12 eV. TDHF calculations are more accurate for two valence electron systems (Na_2 and Na_3^+) where there are no valence screening electrons. Both methods generally yield good agreement with full CI calculations and experimental measurements of photoabsorption spectra for these systems.

Results of TDHF and BSE calculations for Na_8 were compared to experiment and MRD-CI calculations which used effective core potentials and a less extensive basis set and were also in qualitative agreement with both. Calculations for Na_{20} were performed for a C_s symmetry cluster which had been believed to be the ground state of this cluster. A recent particle swarm optimization technique has been used to find a structure for Na_{20} with C_3 symmetry and a lower energy [66]. TDHF and BSE calculations for these clusters are both in good agreement with the experimentally measured photoabsorption spectrum for Na_{20} [85]. There is one clear collective excitation in each TDHF or BSE calculation, but there is no evidence from these calculations of an incipient volume plasmon [85] above 4 eV.

TDHF and BSE are both conserving methods in the sense of Baym and Kadanoff [42]. Both method yield total valence electron oscillator strengths in good agreement with TRK sum rule values. However, TDA approximations to these methods yield gross overestimates to TRK sum rule values. It is speculated that this is because valence electrons in simple metal clusters are strongly correlated (compared to, say, covalently bonded organic molecules). An analysis of the correspondence between TDHF and a CCD method shows that the Y part of eigenvectors of the TDHF equations is closely related to the CCD T double excitation amplitudes, which is relatively important in strongly correlated systems. Omission of Y in TDA calculations may result in overestimation of dipole oscillator strengths and gross violation of the TRK sum rules.

ACKNOWLEDGMENTS

The author wishes to acknowledge helpful discussions with D. Rai and A. Shukla, authors of Ref. [12]. Calculations were performed on the Kelvin and Boyle clusters maintained by the Trinity Centre for High Performance Computing, funded through grants from Science Foundation Ireland and the Irish Higher Education Authority.

[1] X. Blase and C. Attaccalite, Appl. Phys. Lett. **99**, 171909 (2011).
[2] T. Rangel, S. M. Hamed, F. Bruneval, and J. B. Neaton, J. Chem. Theory Comput. **12**, 2834 (2016).
[3] T. Rangel, S. M. Hamed, F. Bruneval, and J. B. Neaton, J. Chem. Phys. **146**, 194108 (2017).
[4] X. Blase, I. Duchemin, and D. Jacquemin, Chem. Soc. Rev. **47**, 1022 (2017).
[5] F. Aryasetiawan and O. Gunnarsson, Rep. Prog. Phys. **61**, 237 (1998).
[6] M. Rohlfing and S. G. Louie, Phys. Rev. Lett. **81**, 2312 (1998).
[7] G. Onida, L. Reining, and A. Rubio, Rev. Mod. Phys. **74**, 601 (2002).
[8] M. Palummo, O. Pulci, R. DelSole, A. Marini, P. Hahn, W. G. Schmidt, and F. Bechstedt, J. Phys.: Condens. Matter **16**, S4313 (2004).
[9] D. Jacquemin, I. Duchemin, and X. Blase, J. Chem. Theory Comput. **11**, 3290 (2015).
[10] C. Azarias, C. Habert, S. Budzák, X. Blase, and I. Duchemin, J. Phys. Chem. A **121**, 6122 (2017).
[11] Q. Ou and J. E. Subotnik, J. Chem. Theory Comput. **14**, 527 (2017).
[12] P. K. Priya, D. K. Rai, and A. Shukla, Eur. Phys. J. D **71**, 116 (2017).
[13] C. H. Patterson (unpublished).
[14] V. Bonačić-Koutecký, P. Fantucci, and J. Koutecký, Chem. Phys. Lett. **166**, 32 (1990).
[15] W. Ekardt, Phys. Rev. B **31**, 6360 (1985).
[16] W. Ekardt and J. M. Pacheco, Phys. Rev. B **52**, 16864 (1995).
[17] M. Madjet, C. Guet, and W. R. Johnson, Phys. Rev. A **51**, 1327 (1995).
[18] F. Calvayrac, E. Suraud, and P.-G. Reinhard, Ann. Phys. **255**, 125 (1997).
[19] J. M. Pacheco and J. L. Martins, J. Chem. Phys. **106**, 6039 (1997).
[20] S. Kümmel, M. Brack, and P.-G. Reinhard, Phys. Rev. B **62**, 7602 (2000).
[21] M. Moseler, H. Häkkinen, and U. Landman, Phys. Rev. Lett. **87**, 053401 (2001).
[22] Y.-P. Zhang, F.-S. Zhang, K.-L. Meng, and G.-Q. Xiao, Commun. Theor. Phys. **47**, 901 (2007).
[23] M. A. L. Marques, A. Castro, and A. Rubio, J. Chem. Phys. **115**, 3006 (2001).
[24] A. Tsolakidis, D. Sánchez-Portal, and R. M. Martin, Phys. Rev. B **66**, 235416 (2002).
[25] M. B. Torres and L. C. Balbás, J. Phys.: Condens. Matter **14**, 5795 (2002).
[26] J.-O. Joswig, L. O. Tunturivuori, and R. M. Nieminen, J. Chem. Phys. **128**, 014707 (2008).
[27] C. Yannouleas, R. A. Broglia, M. Brack, and P. F. Bortignon, Phys. Rev. Lett. **63**, 255 (1989).
[28] V. Kresin, Phys. Rev. B **42**, 3247 (1990).
[29] C. Yannouleas and R. A. Broglia, Phys. Rev. A **44**, 5793 (1991).
[30] C. Guet and W. R. Johnson, Phys. Rev. B **45**, 11283 (1992).
[31] G. Onida, L. Reining, R. W. Godby, R. D. Sole, and W. Andreoni, Phys. Rev. Lett. **75**, 818 (1995).
[32] L. Reining, O. Pulci, M. Palummo, and G. Onida, Int. J. Quantum Chem. **77**, 951 (2000).
[33] G. Pal, Y. Pavlyukh, H. C. Schneider, and W. Hübner, Eur. Phys. J. B **70**, 483 (2009).
[34] Y. Noguchi and K. Ohno, Phys. Rev. A **81**, 045201 (2010).
[35] G. Pal, G. Lefkidis, H. C. Schneider, and W. Hübner, J. Chem. Phys. **133**, 154309 (2010).
[36] Y. Noguchi, K. Ohno, I. Solovyev, and T. Sasaki, Phys. Rev. B **81**, 165411 (2010).
[37] R. Kuwahara, Y. Noguchi, and K. Ohno, Phys. Rev. B **94**, 121116(R) (2016).
[38] T. Sander, E. Maggio, and G. Kresse, Phys. Rev. B **92**, 045209 (2015).
[39] W. Thomas, Naturwissenschaften **13**, 627 (1925).
[40] F. Reiche and W. Thomas, Z. Phys. **34**, 510 (1925).
[41] W. Thomas, Z. Phys. **33**, 408 (1925).
[42] G. Baym and L. P. Kadanoff, Phys. Rev. **124**, 287 (1961).

[43] M. Grüning, A. Marini, and X. Gonze, Nano Lett. **9**, 2820 (2009).
[44] P.-G. Reinhard, O. Genzken, and M. Brack, Ann. Phys. **508**, 576 (1996).
[45] W. de Heer, Rev. Mod. Phys. **65**, 611 (1993).
[46] W. D. Knight, K. Clemenger, W. A. de Heer, W. A. Saunders, M. Y. Chou, and M. L. Cohen, Phys. Rev. Lett. **52**, 2141 (1984).
[47] W. D. Knight, K. Clemenger, W. A. de Heer, and W. A. Saunders, Phys. Rev. B **31**, 2539 (1985).
[48] J. Bowlan, A. Liang, and W. A. de Heer, Phys. Rev. Lett. **106**, 043401 (2011).
[49] M. Broyer, G. Delacrétaz, P. Labastie, J. P. Wolf, and L. Wöste, Phys. Rev. Lett. **57**, 1851 (1986).
[50] W. A. de Heer, K. Selby, V. Kresin, J. Masui, M. Vollmer, A. Chatelain, and W. D. Knight, Phys. Rev. Lett. **59**, 1805 (1987).
[51] K. Selby, M. Vollmer, J. Masui, V. Kresin, W. A. de Heer, and W. D. Knight, Phys. Rev. B **40**, 5417 (1989).
[52] M. Schmidt and H. Haberland, Eur. Phys. J. D **6**, 109 (1999).
[53] C. R. Wang, S. Pollack, D. Cameron, and M. M. Kappes, J. Chem. Phys. **93**, 3787 (1990).
[54] K. Selby, V. Kresin, J. Masui, M. Vollmer, W. A. de Heer, A. Scheidemann, and W. Knight, Z. Phys. D **19**, 43 (1991).
[55] C. Ellert, M. Schmitt, C. Schmitt, T. Reiners, and H. Haberland, Phys. Rev. Lett. **75**, 1731 (1995).
[56] M. Schmidt, C. Ellert, W. Kronmüller, and H. Haberland, Phys. Rev. B **59**, 10970 (1999).
[57] J. L. Martins, J. Buttet, and R. Car, Phys. Rev. B **31**, 1804 (1985).
[58] L. Kronik, I. Vasiliev, M. Jain, and J. R. Chelikowsky, J. Chem. Phys. **115**, 4322 (2001).
[59] V. Bonačić-Koutecký, P. Fantucci, and J. Koutecký, Phys. Rev. B **37**, 4369 (1988).
[60] I. A. Solov'yov, A. V. Solov'yov, and W. Greiner, Phys. Rev. AS **65**, 053203 (2002).
[61] Y. M. Chang, X. Lu, and H. W. K. Tom, J. Chem. Phys. **120**, 6487 (2004).
[62] V. Bonačić-Koutecký, M. M. Kappes, P. Fantucci, and J. Koutecký, Chem. Phys. Lett. **170**, 26 (1990).
[63] V. Bonačić-Koutecký, P. Fantucci, and J. Koutecký, J. Chem. Phys. **93**, 3802 (1990).
[64] V. Bonačić-Koutecký, P. Fantucci, and J. Koutecký, Chem. Rev. **91**, 1035 (1991).
[65] F. Calvo, S. Tran, S. A. Blundell, C. Guet, and F. Spiegelmann, Phys. Rev. B **62**, 10394 (2000).
[66] W. G. Sun, J. J. Wang, C. Lu, X. X. Xia, X. Y. Kuang, and A. Hermann, Inorg. Chem. **56**, 1241 (2017).
[67] U. Röthlisberger and W. Andreoni, J. Chem. Phys. **94**, 8129 (1991).
[68] I. Tamm, J. Phys. (USSR) **9**, 449 (1945).
[69] S. Dancoff, Phys. Rev. **78**, 382 (1950).
[70] C. H. Patterson, Mol. Phy. **108**, 3181 (2010).
[71] L. E. McMurchie and E. R. Davidson, J. Comput. Phys. **26**, 218 (1978).
[72] F. Weigend, A. Köhn, and C. Hättig, J. Chem. Phys. **116**, 3175 (2002).
[73] A. McLean and G. Chandler, J. Chem. Phys. **72**, 5639 (1980).
[74] D. Feller, J. Comput. Chem. **17**, 1571 (1996).
[75] K. L. Schuchardt, B. T. Didier, T. Elsethagen, L. Sun, V. Gurumoorthi, J. Chase, J. Li, and T. L. Windus, J. Chem. Inf. Model **47**, 1045 (2007).
[76] S. Webb, Theor. Chem. Acc. **116**, 355 (2006).
[77] M. W. Schmidt, K. K. Baldridge, J. A. Boatz, S. T. Elbert, M. S. Gordon, J. H. Jensen, S. Koseki, N. Matsunaga, K. A. Nguyen, S. Su, T. L. Windus, M. Dupuis, and J. A. Montgomery, J. Comput. Chem. **14**, 1347 (1993).
[78] M. S. Gordon and M. W. Schmidt, *Theory and Applications of Computational Chemistry: The First Forty Years*, edited by C. E. Dykstra, G. Frenking, K. S. Kim, and G. E. Scuseria (Elsevier, Amsterdam, 2005).
[79] P. Kusch and M. M. Hessel, J. Chem. Phys. **63**, 4087 (1975).
[80] R. F. Barrow, N. Travis, and C. V. Wright, Nature (London) **187**, 141 (1960).
[81] See Supplemental Material at http://link.aps.org/supplemental/10.1103/PhysRevMaterials.3.043804 for additional tables of excitation energies, BSE-TDA and TDHF-TDA spectra of Na_2 and the density of states of Na_{20}.
[82] C. R. Wang, S. Pollack, T. A. Dahlseid, G. M. Koretsky, and M. M. Kappes, J. Chem. Phys. **96**, 7931 (1992).
[83] C. Gatti, S. Polezzo, and P. Fantucci, Chem. Phys. Lett. **175**, 645 (1990).
[84] S. Pollack, C. R. C. Wang, and M. M. Kappes, J. Chem. Phys. **94**, 2496 (1991).
[85] C. Xia, C. Yin, and V. V. Kresin, Phys. Rev. Lett. **102**, 156802 (2009).
[86] V. Bonačić-Koutecký, P. Fantucci, C. Fuchs, C. Gatti, J. Pittner, and S. Polezzo, Chem. Phys. Lett. **213**, 522 (1993).
[87] M.-S. Lee, S. Chacko, and D. G. Kanhere, J. Chem. Phys. **123**, 164310 (2005).
[88] A. Aguado and O. Kostko, J. Chem. Phys. **134**, 164304 (2011).
[89] A. Dreuw and M. Head-Gordon, Chem. Rev. **105**, 4009 (2005).
[90] G. E. Scuseria, T. M. Henderson, and D. C. Sorensen, J. Chem. Phys. **129**, 231101 (2008).
[91] M. H. McAdon and W. A. Goddard, Phys. Rev. Lett. **55**, 2563 (1985).